Journal of Experimental Botany, Vol. 65, No. 18, pp. 5385–5400, 2014
doi:10.1093/jxb/eru297 Advance Access publication 18 July, 2014

Journal of Experimental Botany
www.jxb.oxfordjournals.org

RESEARCH PAPER

Overexpression of a novel *Arabidopsis* PP2C isoform, AtPP2CF1, enhances plant biomass production by increasing inflorescence stem growth

Hiroki Sugimoto[1], Satoshi Kondo[2], Tomoko Tanaka[1], Chie Imamura[1], Nobuhiko Muramoto[1], Etsuko Hattori[2], Ken'ichi Ogawa[3], Norihiro Mitsukawa[1,2,*] and Chikara Ohto[2]

[1] Biotechnology Laboratory, Frontier Research Center, Toyota Central R&D Labs. Inc., 41-1, Yokomichi, Nagakute, Aichi 480-1192, Japan
[2] Bio Research Laboratory, Toyota Motor Corporation, 1, Toyota-cho, Toyota 471-8572, Japan
[3] Research Institute for Biological Sciences (RIBS), Kibichuo-cho, Okayama 716-1241, Japan

* To whom correspondence should be addressed. E-mail: mitsukawa@mosk.tytlabs.co.jp

Received 21 April 2014; Revised 10 June 2014; Accepted 12 June 2014

Abstract

In contrast to mammals, higher plants have evolved to express diverse protein phosphatase 2Cs (PP2Cs). Of all *Arabidopsis thaliana* PP2Cs, members of PP2C subfamily A, including ABI1, have been shown to be key negative regulators of abscisic acid (ABA) signalling pathways, which regulate plant growth and development as well as tolerance to adverse environmental conditions. However, little is known about the enzymatic and signalling roles of other PP2C subfamilies. Here, we report a novel *Arabidopsis* subfamily E PP2C gene, *At3g05640*, designated *AtPP2CF1*. *AtPP2CF1* was dramatically expressed in response to exogenous ABA and was expressed in vascular tissues and guard cells, similar to most subfamily A PP2C genes. *In vitro* enzymatic activity assays showed that AtPP2CF1 possessed functional PP2C activity. However, yeast two-hybrid analysis revealed that AtPP2CF1 did not interact with PYR/PYL/RCAR receptors or three SnRK2 kinases, which are ABI1-interacting proteins. This was supported by homology-based structural modelling demonstrating that the putative active- and substrate-binding site of AtPP2CF1 differed from that of ABI1. Furthermore, while overexpression of *ABI1* in plants induced an ABA-insensitive phenotype, *Arabidopsis* plants overexpressing *AtPP2CF1* (*AtPP2CF1oe*) were weakly hypersensitive to ABA during seed germination and drought stress. Unexpectedly, *AtPP2CF1oe* plants also exhibited increased biomass yield, mainly due to accelerated growth of inflorescence stems through the activation of cell proliferation and expansion. Our results provide new insights into the physiological significance of *AtPP2CF1* as a candidate gene for plant growth production and for potential application in the sustainable supply of plant biomass.

Key words: ABA (abscisic acid); biomass; cell proliferation and expansion; inflorescence stem; plant; PP2C.

Introduction

Protein phosphatase 2Cs (PP2Cs) are monomeric enzymes in which catalytic and regulatory domains are present on the same polypeptide, and which require divalent metal ions (typically Mn^{2+} or Mg^{2+}) for their activity. PP2Cs play important roles in cell differentiation, growth, and metabolism, and in environmental stress signalling pathways, and are found in eukaryotes and some prokaryotes (Cohen, 1994; Schweighofer *et al.*, 2004; Lu and Wang, 2008; Shi, 2009). While at least 18 PP2Cs have been identified in mammalian cells, plant PP2Cs are part of a larger and more diverse family

Abbreviations: ABA, abscisic acid; GUS, β-glucuronidase; PP2C, protein phosphatase 2C; PSP, Ser/Thr phosphatase; PTP, Try phosphatase.

of manganese/magnesium-dependent protein phosphatases (PPMs), with 80 isoforms identified to date in *Arabidopsis* and 90 in rice (*Oryza sativa*), implying that plant PP2C isoforms possess unique patterns of tissue and subcellular localization associated with diverse functions (Xue *et al.*, 2008; Singh *et al.*, 2010).

The plant hormone abscisic acid (ABA) regulates various aspects of plant growth and development, including seed maturation, dormancy, and tolerance to adverse environmental conditions—particularly drought, cold, and salinity (Verslues and Zhu, 2007; Cutler *et al.*, 2010). Among the 13 subfamilies of *Arabidopsis* PP2C isoforms (A–L) classified based on phylogenetic analysis (Xue *et al.*, 2008), members of subfamily A have been shown to be key negative regulators of ABA signalling pathways (Cutler *et al.*, 2010; Hubbard *et al.*, 2010; Hauser *et al.*, 2011; Joshi-Saha *et al.*, 2011). Considerable progress in biochemical and structural investigations of subfamily A PP2Cs has advanced the understanding of their molecular function in ABA signalling pathways. In the absence of ABA, members of this subfamily including ABI1, ABI2, and HAB1 dephosphorylate three members of the Snf1-related protein kinase 2 (SnRK2) family (SnRK2.2, -2.3, and -2.6), maintaining them in an inactive state. Under stress conditions, the presence of increased ABA is recognized by intracellular ABA receptors, namely the PYR/PYL/RCAR family of START proteins. These ABA-bound receptors bind to the catalytic site of subfamily A PP2Cs and inhibit their phosphatase activity, permitting the activation of SnRK2 kinases. In turn, SnRK2 kinases phosphorylate downstream factors such as the AREB/ABF transcription factors required for activation of ABA-responsive genes and SLAC1 anion channels involved in stomatal closure, thus relaying ABA signals (Cutler *et al.*, 2010; Hubbard *et al.*, 2010; Hauser *et al.*, 2011; Joshi-Saha *et al.*, 2011).

Plant subfamily E PP2Cs constitute the largest of the subfamilies (Supplementary Fig. S1) (Xue *et al.*, 2008). A unique characteristic of subfamily E PP2Cs is the insertion of two amino acids in the β3-α1 loop of consensus motif 4, corresponding to residues 171–185 of ABI1 and comprising an important part of the active and substrate-binding sites (Supplementary Fig. S2) (Xue *et al.*, 2008; Ma *et al.*, 2009; Melcher *et al.*, 2009; Miyazono *et al.*, 2009; Nishimura *et al.*, 2009, 2010; Park *et al.*, 2009; Santiago *et al.*, 2009; Yin *et al.*, 2009). Dominant mutations in subfamily A PP2Cs, such as *abi1-1* and *abi2-1*, which inhibit binding to PYR/PYL/RCAR receptors and induce the ABA-insensitive phenotype, reside within the β3-α1 loop, highlighting not only the general importance of this loop for substrate recognition and specificity (Miyazono *et al.*, 2009; Umezawa *et al.*, 2009), but also the functional differences between subfamily E PP2Cs and other PP2Cs. However, despite the potential physiological importance of subfamily E PP2Cs, much less is known about their enzymatic and signalling roles.

In this study, we characterized a novel PP2C family protein (designated AtPP2CF1) that can be classified as a subfamily E PP2C. Of the subfamily E members, *AtPP2CF1* expression was strongly upregulated by ABA. An *in vitro* enzymatic assay revealed that AtPP2CF1 had serine/threonine phosphatase (PSP) activity typical of a classical PP2C, indicating that its activity was dependent on Mg^{2+}. *AtPP2CF1* exhibited an expression pattern similar to that of subfamily A PP2Cs such as *ABI1*, with transcripts detected in vascular tissues and stomatal guard cells. However, using a yeast two-hybrid (Y2H) system and homology-based structural modelling of AtPP2CF1, we found that AtPP2CF1 was unable to bind PYR/PYL/RCAR receptors or three SnRK2 kinases, both of which are ABI1-interacting proteins. Furthermore, overexpression of *AtPP2CF1* caused *Arabidopsis* plants to exhibit weak hypersensitivity to ABA, which differed from the effect observed with overexpression of *ABI1* and unexpectedly resulted in increased biomass production.

Materials and methods

Plant materials and growth conditions

All *Arabidopsis thaliana* plants used in this study, including wild-type, *phyB-9* single mutants (*phyB*), *cry2-1 phyB-9* double mutants (*cry2 phyB*), and transgenic lines, were of the Columbia ecotype (Mockler *et al.*, 1999). Seeds were sown aseptically on Murashige and Skoog (MS) solid medium [0.5% (w/v) gellan gum or 0.8% (w/v) agar] with or without 1% sucrose or on soil Supermix A (Sakata, Kanagawa, Japan). After stratification for 3 d at 4°C, plants were grown in a growth chamber [22°C and approximately 60% relative humidity (RH)] under long-day conditions (16-h light/8-h dark cycle, approximately 50 μmol m^{-2} s^{-1} white fluorescent light). Seedlings of plants grown on solid medium were transferred to soil at 21 d after germination and fertilized weekly with Hyponex (1:1000 dilution; Hyponex Japan, Osaka, Japan).

Real-time quantitative PCR (RT-qPCR)

Total RNA was isolated using an RNeasy Plant Mini Kit (Qiagen, Valencia, CA, USA), and on-column DNase treatment was performed using an RNase-Free DNase Set (Qiagen, Hilden, Germany). cDNA was generated using a High Capacity RNA-to-cDNA Kit (Applied Biosystems, Foster City, CA) and subjected to RT-qPCR amplification using the Power SYBR Green PCR Master Mix (Applied Biosystems, Warrington, UK). Quantification of RT-qPCR reactions was conducted using an ABI Prism 7000 sequence detection system and ABI Prism 7000 SDS software (Applied Biosystems) with gene-specific primers (Supplementary Table S1).

Construction of transgenic Arabidopsis *plants*

Protocols for the construction of plasmids are provided in Supplementary Methods S1 and S2. *Arabidopsis* transformation was carried out by the floral dip method (Clough and Bent, 1998).

Histochemical analysis of GUS staining

Arabidopsis seedlings were harvested into ice-cold 90% (v/v) acetone, incubated at room temperature for 20 min to permeabilize the tissue, and then washed three times with 50 mM sodium phosphate buffer, pH 7.0. β-glucuronidase (GUS) reactions were performed in GUS staining buffer [1.9 mM 5-bromo-4-chloro-3-indolyl-β-D-glucuronide-cyclohexylammonium salt, 0.5 mM $K_3Fe(CN)_6$, 0.5 mM $K_4[Fe(CN)_6]\cdot 3H_2O$, 0.3% Triton X-100, and 50 mM sodium phosphate buffer, pH 7.0]. Samples were infiltrated under a vacuum for 5 min and then incubated overnight at 37°C. The GUS-staining buffer was removed and the samples were washed and cleared in 70% ethanol. Observations were made with a stereomicroscope (SZX12; Olympus, Tokyo, Japan) and a fluorescence microscope (Biorevo BZ-9000; Keyence, Osaka, Japan).

Yeast ptc1 *complementation test*

The diploid *Saccharomyces cerevisiae* strain BY4743 (MATa/α his3Δ1/his3Δ1 leu2Δ0/leu2Δ0 lys2Δ0/LYS2 MET15/met15Δ0 ura3Δ0/ura3Δ0) was used in this study. The *ptc1* single-knockout mutant strains were generated by the Saccharomyces Genome Deletion Project (Winzeler *et al.*, 1999) and obtained from Open Biosystems (Huntsville, AL, USA). Protocols describing the construction of plasmids for the yeast complementation test are provided in Supplementary Methods S1 and S3. Yeast cells were grown and maintained in minimal synthetic medium containing either glucose (SD) or galactose (SG), or in complete medium containing either glucose (YPD) or galactose (YPG).

Purification of AtPP2CF1 and PP2C activity assays

Protocols detailing the construction of *pGEX GST-AtPP2CF1* and *pGEX GST-ABI1* are provided in Supplementary Methods S1 and S4. These constructs were introduced into *Escherichia coli* BL21 (Novagen, Madison, WI, USA). Recombinant fusion proteins were purified using a GSTrap 4B column (GE Healthcare, Uppsala, Sweden), concentrated with a Vivaspin 20 centrifugal concentrator (10 000 molecular weight cutoff; Sartorius, Goettingen, Germany), and passed through a PD-10 desalting column (GE Healthcare) to remove free glutathione, according to the manufacturer's instructions. Protein concentrations were determined using the Pierce 660 nm Protein Assay Kit (Thermo Scientific, Rockford, IL, USA).

PP2C activities were measured using separate Ser/Thr and Tyr phosphatase assay systems (Promega, Madison, WI), according to the manufacturer's instructions. Briefly, the reactions were performed in 100 µl of assay buffer [50 mM imidazole (pH 7.2), 0.2 mM EGTA, 5 mM $MgCl_2$, 0.02% β-mercaptoethanol, and 0.1 mg ml^{-1} BSA] by using 100 µM chemically synthesized phosphopeptide substrate [PSP substrate RRA(pT)VA, where pT represents phosphothreonine; or the tyrosine phosphatase (PTP) substrates END(pY)INASL or DADE(pY)LIPQQG, where pY represents phosphotyrosine] and 50–5250 ng of recombinant protein (GST-AtPP2CF1 or GST-ABI1). The inhibitors used in the study were NaF (50 mM), $NaVO_3$ (1 mM), EDTA (10 mM), and okadaic acid (10 µM). For EDTA, the indicated concentrations of the chelator were added to the reaction mixtures without $MgCl_2$. Absorbance was measured at 650 nm in an Infinite F5000 microplate reader (Tecan Austria, Grödlg, Austria).

Homology-based structural modelling of AtPP2CF1

A homology-based model of AtPP2CF1 was built using the Build Homology Models protocol in Discovery Studio 3.1 (Accelrys, San Diego, CA, USA). The crystal coordinates of ABI1 in the PYL1-(+)-ABA-ABI1 complex (Protein Data Bank code 3kdj) were used as a template. Sequence alignment of AtPP2CF1 and ABI1 was made based on their structural superimposition and was adjusted by hand. Model quality was evaluated using the Profiles 3D protocol in Discovery Studio 3.1; the model structure with the highest Verify score (93.94, expected high score = 132.384) was selected as the most reliable model of AtPP2CF1.

Germination assays and leaf water loss measurements

For germination assays, ~60 sterilized seeds were plated on MS agar medium with increasing concentrations of (±)-ABA (Sigma-Aldrich, St Louis, MO, USA). After stratification for 4 d at 4°C, seedlings were grown in a growth chamber under long-day conditions. To determine seed germination rates, seeds that had germinated and developed green and expanded cotyledons were scored in six independent experiments. Leaf water loss was measured using the detached aerial parts of 3-week-old seedlings. Five seedlings per line were cut above the hypocotyl and fresh weight (FW) was determined under growth chamber conditions at the indicated times in three independent experiments.

Histological observation of inflorescence stems

For transverse sections, basal parts of 10- to 15-cm-long primary inflorescence stems or those of 9-week-old plants (10 or 20 mm from the rosette base, respectively) were embedded in agarose blocks and sectioned into 100-µm-thick slices using a microslicer (DTK-1000; Dosaka, Kyoto, Japan). The sections were incubated with 0.05% (w/v) toluidine blue at room temperature for 1 min, washed, and then observed using a fluorescence microscope (Biorevo BZ-9000; Keyence, Osaka, Japan). The images were processed and assembled with Adobe Photoshop (Adobe Systems, CA, USA). For each stem, the diameter and area imaged were measured using Paint.NET (http://www.getpaint.net/).

For observation of stem epidermal cells, the stem epidermis was peeled from the basal parts (20 mm from the rosette base) of primary inflorescence stems in 9-week-old plants, incubated with 0.01% (w/v) safranin at room temperature for 1 min, washed, and then observed using a fluorescence microscope (Keyence).

Dry biomass measurement

Arabidopsis plants were grown on soil in a growth chamber under long-day conditions for 12 weeks and fertilized weekly with Hyponex (1:500 dilution). At 12 weeks, the plants were maintained without watering for two weeks and were then cut at their hypocotyls. Dry seeds and plant tissues (excluding roots) were weighed separately on an XS205 Dual Range analytical balance (Mettler Toledo, Greifensee, Switzerland).

Measurement of flowering time

Flowering time was determined as both 'days to flowering' and 'leaf number'. Days to flowering was determined as the number of days from sowing until the first flower bud became visible. Leaf number was determined by counting the number of rosette leaves at the time when the first flower bud became visible.

Accession numbers

The Arabidopsis Genome Initiative (AGI) numbers from The Arabidopsis Information Resource (TAIR) database (http://www.arabidopsis.org/) are as follows: *At3g05640* (*AtPP2CF1*), *At4g26080* (*ABI1*), *At4g17870* (*PYR1*), *At5g46790* (*PYL1*), *At2g26040* (*PYL2*), *At1g73000* (*PYL3*), *At2g38310* (*PYL4*), *At5g05440* (*PYL5*), *At2g40330* (*PYL6*), *At4g01026* (*PYL7*), *At5g53160* (*PYL8*), *At1g01360* (*PYL9*), *At4g27920* (*PYL10*), *At5g45860* (*PYL11*), *At5g45870* (*PYL12*), *At4g18620* (*PYL13*), *At3g50500* (*SnRK2.2*), *At5g66880* (*SnRK2.3*), *At4g33950* (*SnRK2.6*)

Results

AtPP2CF1 *gene expression increased dramatically in response to exogenous ABA*

In *Arabidopsis*, most subfamily A PP2C genes and several subfamily B and G PP2C genes are transcriptionally activated by ABA (Leung *et al.*, 1997; Merlot *et al.*, 2001; Saez *et al.*, 2004; Kuhn *et al.*, 2006; Nishimura *et al.*, 2007; Brock *et al.*, 2010; Liu *et al.*, 2012; Zhang *et al.*, 2012). Previous microarray analyses have suggested that the expression of a few subfamily E PP2Cs is also induced by exogenous ABA (Goda *et al.*, 2008). Thus, we first investigated whether expression of subfamily E PP2C genes was regulated by exogenous ABA (Fig. 1A). RT-qPCR experiments using total RNA isolated from aerial parts of *Arabidopsis* plants treated with ABA demonstrated that transcripts of four subfamily

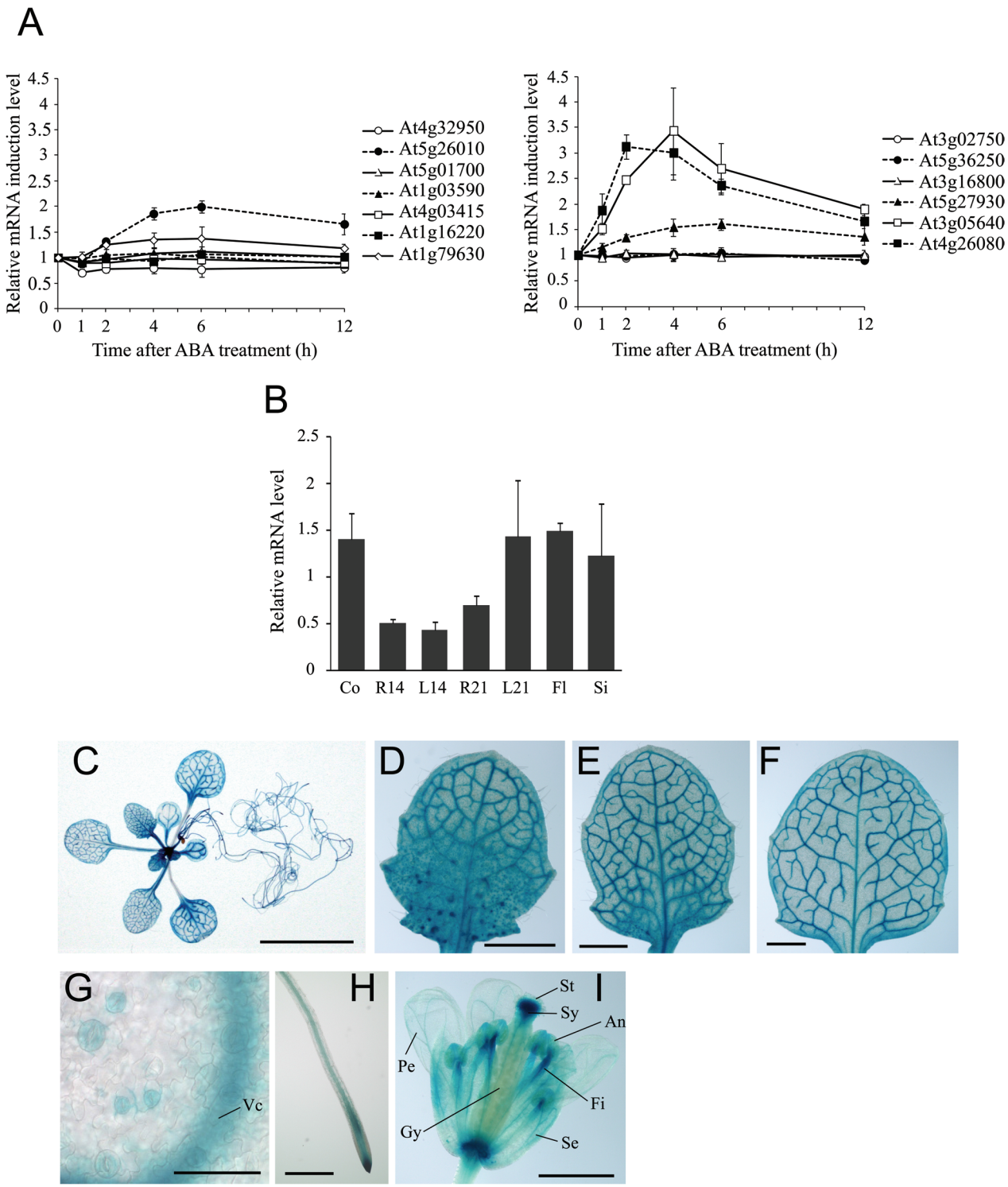

Fig. 1. Spatial, temporal, and ABA-mediated regulation of *AtPP2CF1* expression. *Arabidopsis* plants were germinated aseptically on MS medium with gellan gum. At 21 d after germination, seedlings were transferred to soil. (A) Time course of the induction of subfamily E PP2C mRNA expression in aerial parts of wild-type *Arabidopsis* plants in response to exogenous ABA. Two-week-old seedlings were sprayed with 10 μM ABA or 0.1% DMSO (mock control). Total RNA from aerial parts was isolated at the indicated time points after ABA or mock treatment and subjected to RT-qPCR. The expression ratios of individual subfamily E PP2C genes to *UBC9* were calculated for each time point and treatment (raw data are shown in Supplementary Fig. S3), and induction of each PP2C mRNA after ABA treatment was calculated by dividing the expression after ABA treatment by the expression after mock treatment at each time point. Values represent the mean ± SD of three independent experiments. (B) Expression of *AtPP2CF1* transcripts. Total RNA from different tissues of wild-type *Arabidopsis* plants was isolated and subjected to RT-qPCR. The expression ratios of *AtPP2CF1* to *UBC9* were calculated for each sample. Values represent the mean ± SD of three independent experiments. Co, 7-d-old cotyledons; R14, 14-d-old roots; L14, 14-d-old first and second rosette leaves; R21, 21-d-old roots; L21, 21-d-old first to fourth rosette leaves; Fl, flowers; Si, siliques. (C–I) Histochemical analysis of GUS activity in *Arabidopsis pAtPP2CF1:GUS* transgenic plants. (C) A 21-d-old seedling. (D–F) A developmental series of rosette leaves ranging from young (D) to old (F) within a 21-d-old transgenic seedling. (G) Guard cells of young leaves. (H) Roots. (I) Flowers. Vc, vascular cylinder; An, anther; Fi, filament, Gy, gynoecium; Pe, petal; Se, sepal; St, stigma; Sy, style. Scale bars: 10 mm (C); 1 mm (D–F, I); 500 μm (H); 50 μm (G).

E genes (*At1g79630*, *At3g05640*, *At5g26010*, and *At5g27930*) accumulated in response to ABA. Interestingly, peak expression of these genes was delayed by ~2–4 h compared with that of *ABI1*, and accumulation of transcripts was downregulated by exogenous ABA only for one subfamily E PP2C gene, *At4g32950* (Fig. 1A). Of the four ABA-inducible subfamily E PP2C genes, *At3g05640* showed the strongest response to ABA, with an induction of at least 3.5-fold (Fig. 1A), indicating its physiological significance in the ABA signal transduction pathway. This gene was designated *AtPP2CF1* and subsequent experiments were focussed on this target.

AtPP2CF1 *expression is subject to developmental and cell-type-specific regulation*

Genomes of higher plants, including *Arabidopsis* and rice, contain a greater number of PP2C genes than mammalian genomes (Schweighofer *et al.*, 2004; Lu and Wang, 2008; Xue *et al.*, 2008; Singh *et al.*, 2010). Therefore, it was reasonable to predict that each plant PP2C gene might exhibit a unique developmental expression pattern based on its physiological function. RT-qPCR analysis revealed that *AtPP2CF1* was ubiquitously expressed in all plant tissues, with higher levels of expression in the cotyledons, mature leaves, flowers, and siliques (Fig. 1B).

In order to examine the tissue- or cell-type-specific expression pattern of *AtPP2CF1* in greater detail, we prepared a construct expressing the GUS reporter gene under the transcriptional control of the *AtPP2CF1* promoter and introduced this into *Arabidopsis* plants (Fig. 1C–I). Vascular-specific GUS staining was detected in most tissues, including the cotyledons, rosette leaves, roots, hypocotyl, sepals, and petals (Fig. 1C–I and Supplementary Fig. S4). *AtPP2CF1* expression was also detectable at low levels in guard cells (Fig. 1G). These tissues and cells corresponded to the sites of ABA synthesis, consistent with the ability of ABA to induce *AtPP2CF1* expression (Fig. 1A) (Koiwai *et al.*, 2004). Furthermore, GUS staining revealed that *AtPP2CF1* was expressed predominantly in root tips but weakly in the basal regions of young developing leaves, which have high rates of cell division, suggesting that *AtPP2CF1* may play a role in proliferative growth (Fig. 1D–F, H).

AtPP2CF1 *encoded an enzymatically active PP2C-type protein phosphatase*

AtPP2CF1 showed high similarity to yeast PTC1 and *Arabidopsis* ABI1 (33.1% and 36.5%, respectively) (Supplementary Fig. S5). To examine whether AtPP2CF1 had PP2C activity, we carried out a yeast complementation test. In yeast (*S. cerevisiae*), loss of functional PTC1 leads to a temperature-sensitive growth defect in which mutant cells grow more slowly at the restrictive temperature (37°C) than at the permissive temperature (30°C) (Maeda *et al.*, 1993). Therefore, only the yeast *ptc1* knockout strain producing an active PP2C is able to grow normally at the restrictive temperature. In our study, transformation of *ptc1* cells with the PTC1 expression vector restored normal growth at the restrictive temperature (Fig. 2A, construct 2), while transformation with an empty vector did not (Fig. 2A, construct 1). Some reports have demonstrated that expression of some subfamily A PP2C members, including ABI1, could complement the growth defect in this strain (Fig. 2A, construct 4) (Bertauche *et al.*, 1996; Leung *et al.*, 1997; Zhang *et al.*, 2012). However, in the present study, expression of AtPP2CF1 did not restore the temperature-sensitive growth defect of this strain (Fig. 2A, construct 3), suggesting that AtPP2CF1 may not have functional PP2C activity or could not efficiently recognize the original substrates of yeast PTC1.

To verify these possibilities, we assessed the *in vitro* enzymatic activity of AtPP2CF1 using one PSP and two PTP phosphopeptides. An AtPP2CF1 construct with GST fused to the N-terminal region (GST-AtPP2CF1) exhibited high substrate specificity for the PSP phosphopeptide, although this specific activity was approximately 8-fold lower than that of purified GST-tagged ABI1 (GST-ABI1), which was used as a positive control (Fig. 2B, C). Similar to GST-ABI1, the phosphatase activity of GST-AtPP2CF1 was inhibited by NaF, a nonspecific inhibitor of PSPs, but not by okadaic acid or $NaVO_3$, inhibitors of protein phosphatases 1 and 2A (PP1 and PP2A) and PTPs, respectively. Moreover, Mg^{2+} ions were critical for the phosphatase activity of AtPP2CF1 (Fig. 2B). Together with the yeast *ptc1* complementation test, these results suggested that AtPP2CF1 possessed functional PP2C activity but exhibited different substrate specificity from subfamily A PP2Cs.

AtPP2CF1 *is unable to recognize and bind to the interacting proteins of some subfamily A PP2Cs*

Accumulating evidence from Y2H assays indicates that subfamily A PP2Cs can interact with PYR/PYL/RCAR receptors and three SnRK2 kinases (SnRK2.2, -2.3, and -2.6), upstream and downstream regulators of subfamily A PP2Cs, respectively, albeit with different intensities (Ma *et al.*, 2009; Park *et al.*, 2009; Umezawa *et al.*, 2009; Bhaskara *et al.*, 2012; Soon *et al.*, 2012). However, our Y2H assays revealed that AtPP2CF1 did not bind to any of the PYR/PYL/RCAR receptors or SnRK2 kinases tested in this experiment, either in the presence or absence of exogenous ABA (Supplementary Fig. S6), consistent with the different substrate specificities observed for AtPP2CF1 and ABI1 (Fig. 2A).

Next, to gain structural insight into the putative active and substrate-binding sites of AtPP2CF1, homology-based structural modelling of AtPP2CF1 was performed using the previously solved crystal structure of ABI1 in complex with PYL1 and (+)-ABA (Melcher *et al.*, 2009; Miyazono *et al.*, 2009; Nishimura *et al.*, 2009; Yin *et al.*, 2009). Two perpendicular views of the structure of AtPP2CF1 revealed that its catalytic domain adopted an overall conformation similar to that of ABI1 in the PYL1-(+)-ABA-ABI1 complex (Supplementary Figure S7). AtPP2CF1 comprised a central β-sandwich containing two five-stranded antiparallel β-sheets flanked by a pair of α-helices on each side. Notably, at least one metal ion was coordinated by three residues (Asp98, Asp294, and Asp340) in the active site of AtPP2CF1 (corresponding to residues Asp177, Asp347, and Asp413 of ABI1), consistent with the requirement of Mg^{2+} for its PP2C activity (Figs 2B and 3A;

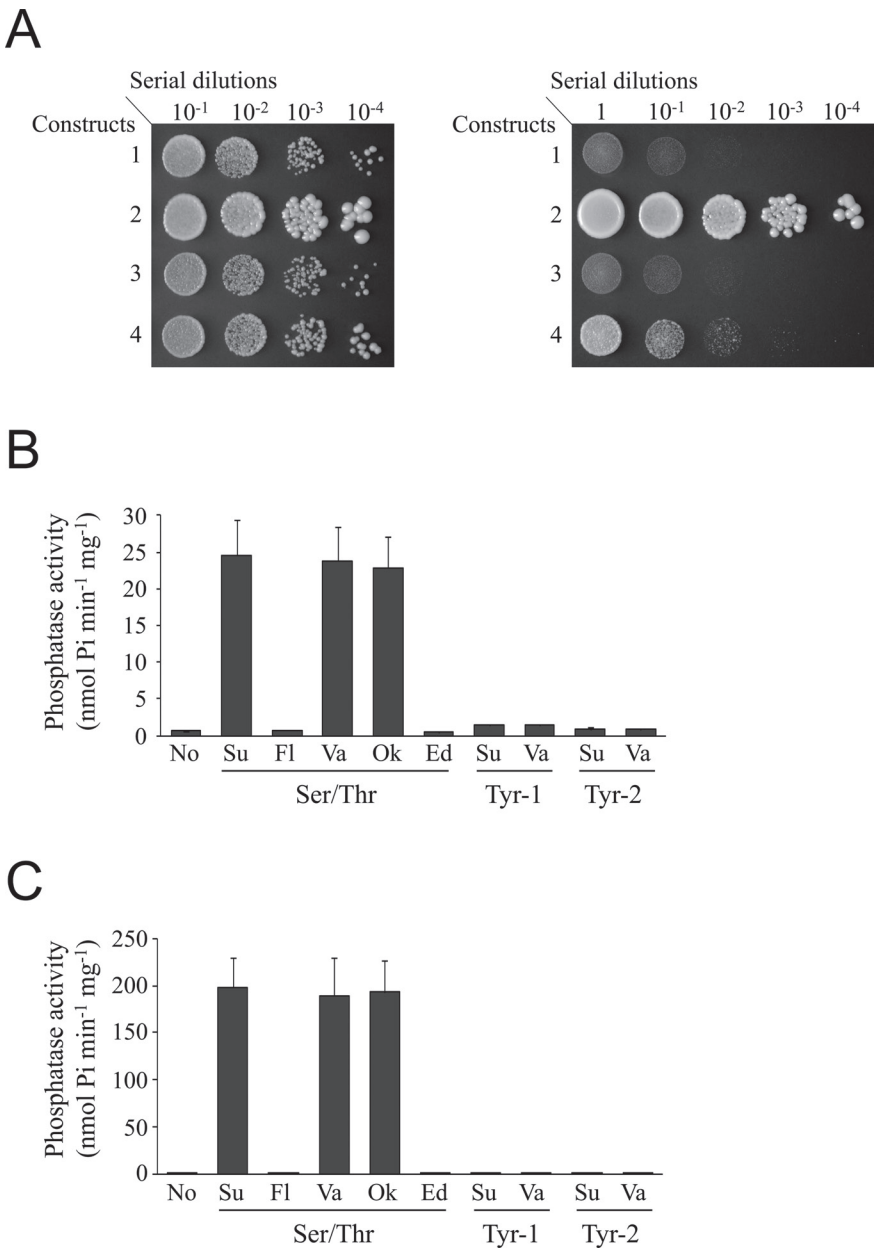

Fig. 2. AtPP2CF1 had functional PP2C activity. (A) Complementation test of the yeast *ptc1* mutation by AtPP2CF1. The yeast *ptc1* knockout strain was transformed with constructs 1 (*pYC2/CT*, empty vector), 2 (*pYC2/CT PTC1*), 3 (*pYC2/CT AtPP2CF1*), or 4 (*pYC2/CT ABI1*) under the control of the galactose-inducible *GAL1* promoter. Serial dilutions of exponentially growing yeast cell cultures were spotted on an SG plate lacking uracil, and growth was observed after 4 d at the permissive temperature (30°C, left) or the restrictive temperature (37°C, right). (B, C) Phosphatase activities of GST-AtPP2CF1 (B) and GST-ABI1 (C). Phosphatase assays were performed as described in the Materials and methods. Purified GST-AtPP2CF1 or GST-ABI1 was incubated with no substrate (No), 100 μM substrate (Su), 100 μM substrate plus 50 mM NaF (Fl), 1 mM $NaVO_3$ (Va), 10 μM okadaic acid (Ok), or 10 mM EDTA (Ed). Values represent the mean ± SD of three independent experiments.

Supplementary Fig. S7). However, AtPP2CF1 exhibited differences within both the active site and catalytic domain residues (Fig. 3A). For example, although the Glu residue (Glu142) in the active site of ABI1 is key to the interaction with PYL1 (Miyazono *et al.*, 2009; Yin *et al.*, 2009), the corresponding residue in AtPP2CF1 was Gln76. Moreover, AtPP2CF1 contained the subfamily E PP2C characteristic insertion of two amino acids in the β3-α1 loop of consensus motif 4, which forms an essential part of the active- and substrate-binding site, causing this loop to protrude over the structure and form a steric hindrance against PYL1 (Fig. 3B; Supplementary Figures S2 and S7). It has been reported that Trp300 of ABI1 is an important residue for both direct interaction with PYR/PYL/RCAR and for recognition of (+)-ABA (Melcher *et al.*, 2009; Miyazono *et al.*, 2009; Yin *et al.*, 2009). Although AtPP2CF1 appeared to have the corresponding Trp residue (Trp246) in a suitable position, the indole ring of Trp246 was significantly rotated compared to the corresponding residue in ABI1 (Trp300), causing steric hindrance that would prevent direct access to (+)-ABA and PYL1 (Fig. 3B; Supplementary Fig. S7). These observations suggested that AtPP2CF1 was no longer able to interact efficiently with R-(+)-ABA-bound

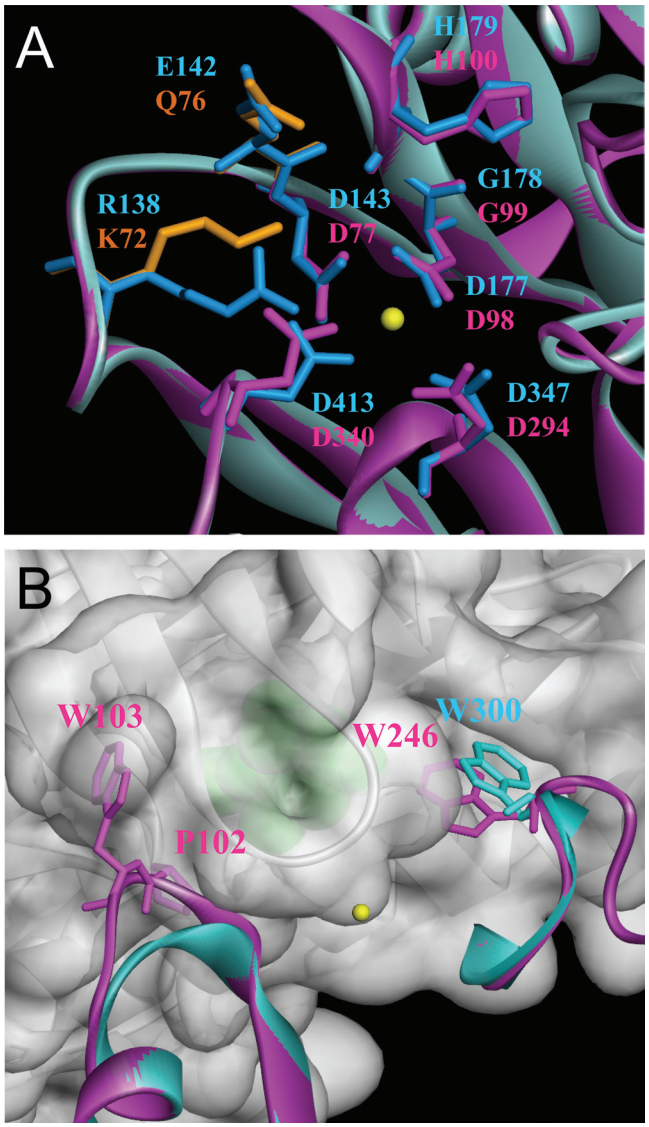

Fig. 3. Homology-based structural modelling of AtPP2CF1. Ribbon representation of AtPP2CF1. (A) Close-up view of the putative active site of AtPP2CF1. The key residues comprising the active site of ABI1 are shown as blue-stick representations. Among the active site residues of AtPP2CF1, residues identical to ABI1 are shown as magenta-stick representations, and those specific for AtPP2CF1 are depicted as orange-stick representations. Note that at least one metal ion (yellow sphere) was bound to the active site of AtPP2CF1. (B) Close-up view of the AtPP2CF1 regions corresponding to the primary-binding interface of ABI1 with PYL1. PYL1 (grey) is shown in a semi-transparent surface representation. (+)-ABA is shown as a green sphere. For simplicity, only two regions of AtPP2CF1 (magenta), which correspond to the β3-α1 loop and the β9-β10 loop of ABI1 (blue), are shown. Trp246 of AtPP2CF1, Trp300 of ABI1, and Pro102 and Trp103 of AtPP2CF1, which correspond to an insertion of two amino acids in the β3-α1 loop of consensus motif 4, are highlighted in the stick representation.

PYR/PYL/RCAR receptors, reinforcing the idea that the substrate specificity of AtPP2CF1 differs from that of subfamily A PP2Cs.

Overexpression of AtPP2CF1 *led to an ABA-hypersensitive phenotype in* Arabidopsis

Next, we investigated whether AtPP2CF1 functioned in ABA signal transduction pathways by generating transgenic *Arabidopsis* plants overexpressing *AtPP2CF1* or *ABI1* under the transcriptional control of their 35SΩ promoters, *AtPP2CF1oe* and *ABI1oe*, respectively (Fig. 4A) and by examining the ABA sensitivities of these plants during seed germination and seedling development. RT-qPCR experiments showed that *AtPP2CF1* transcript accumulation was markedly higher (3.5–7.1-fold) in two independent *AtPP2CF1oe*-line plants (#1 and #2) than in wild-type plants (Fig. 4B). Expression of *ABI1* was also higher (3.4-fold) in *ABI1oe* plants than in wild-type plants (Fig. 4B).

As expected from previous studies (Nishimura *et al.*, 2010), *ABI1oe* plants clearly showed ABA insensitivity in seed germination tests (Fig. 4C). However, *AtPP2CF1oe* plants displayed the opposite phenotype; that is, germination efficiency in two independent *AtPP2CF1oe* plants was reduced to a lesser degree in the presence of exogenous ABA compared with that of wild-type plants, suggesting that *AtPP2CF1oe* plants were weakly hypersensitive to ABA during seed germination (Fig. 4C).

Under drought conditions, regulation of water loss in plants is a crucial ABA-mediated process involved in the stomatal response. We next investigated whether *AtPP2CF1* may be involved in regulating water homeostasis by measuring FW loss in detached aerial parts of plants. Although *ABI1oe* plants showed a significant increase in the rate of water loss compared with the wild-type, two independent *AtPP2CF1oe* plants exhibited weaker reduction in water loss, suggesting the occurrence of ABA-hypersensitive stomatal closure consistent with *AtPP2CF1* gene expression in guard cells (Figs 1G and 4D).

AtPP2CF1oe *plants displayed increased inflorescence stem growth*

Arabidopsis plants that overexpress subfamily A PP2Cs such as *ABI1* and *HAB1* have been reported to exhibit significantly reduced size under moderate RH due to impaired stomatal closure and resulting deficiencies in water retention (Robert *et al.*, 2006; Nishimura *et al.*, 2010). Even under high RH, transgenic plants overexpressing *HAB1* are smaller than corresponding wild-type plants (Robert *et al.*, 2006). Here, under 60% RH, *ABI1oe* plants were smaller than wild-type plants (as expected) and exhibited leaf epinasty (Fig. 4A). In contrast, *AtPP2CF1oe* plants had similar morphology to wild-type plants, with the exception of long petioles (Fig. 4A). Furthermore, *ABI1oe* plants had short inflorescence stems but displayed shoot branching patterns (numbers of rosette and cauline branches) similar to those of wild-type plants (Fig. 5A–G and Supplementary Fig. S8). However, two independent *AtPP2CF1oe* plants developed longer and thicker inflorescence stems (Fig. 5A, B, F, G; Supplementary Fig. S8). There were also significant differences in numbers of shoot branches between wild-type and *AtPP2CF1oe* plants. In *AtPP2CF1oe* plants, a small but significant decrease in numbers of rosette branches was observed (one to two), while cauline branch numbers on the primary inflorescence were increased by one to two (Fig. 5C–E). Thus, overexpression of *AtPP2CF1* resulted in a more erect, robust-stature phenotype

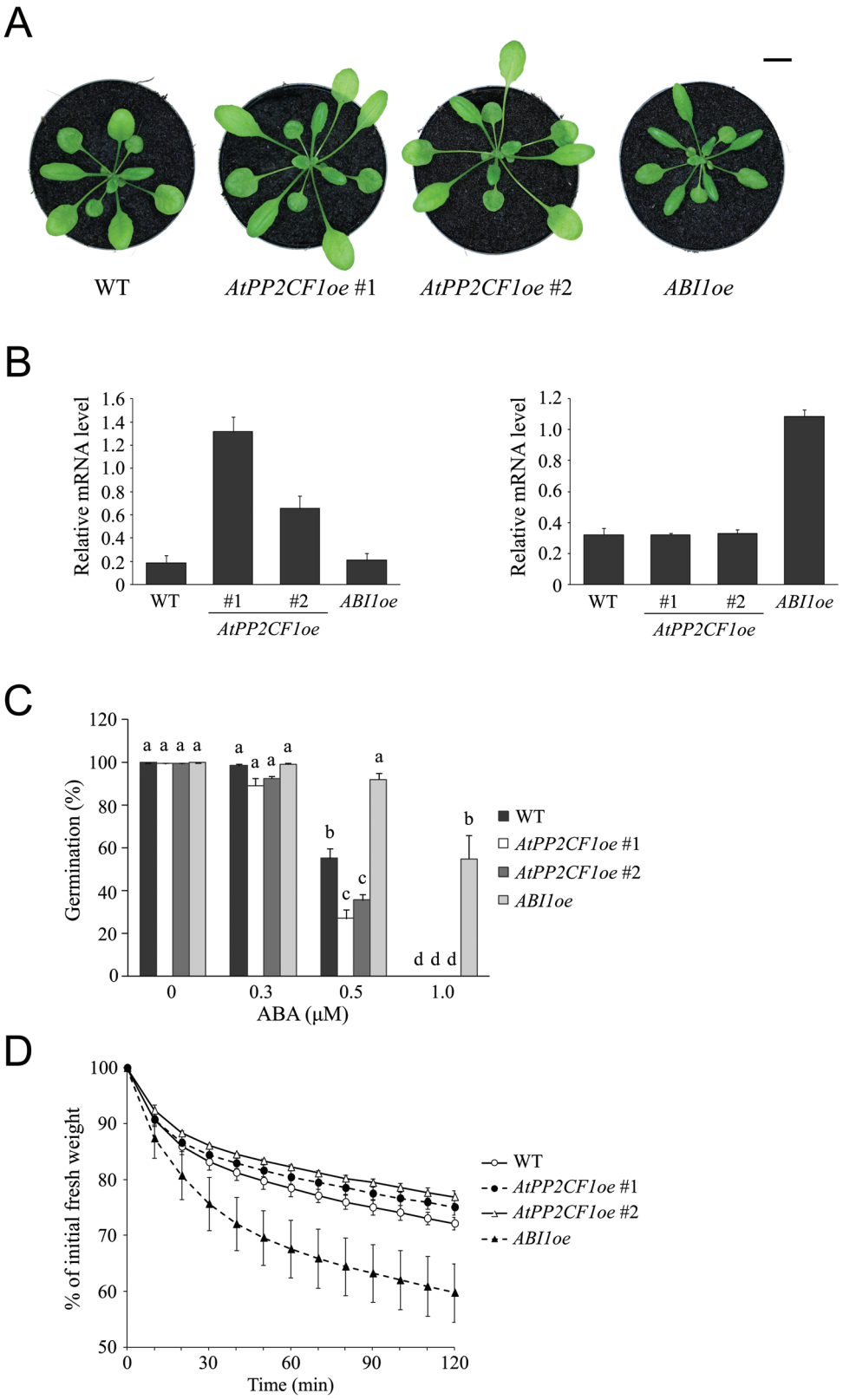

Fig. 4. Phenotypic features of *Arabidopsis AtPP2CF1oe* and *ABI1oe* transgenic plants. (A) 32-d-old wild-type (WT), *AtPP2CF1oe* (#1 and #2), and *ABI1oe* plants. Scale bar: 10 mm. (B) Expression of *AtPP2CF1* (left) and *ABI1* (right) transcripts in *AtPP2CF1oe* or *ABI1oe* plants. Total RNA from aerial parts of 2-week-old seedlings grown aseptically on MS medium with gellan gum was isolated and subjected to RT-qPCR. The expression ratios of *AtPP2CF1* and *ABI1* to *UBC9* were calculated for each sample. Values represent the mean ± SD of three independent experiments. (C) Seed germination rate of WT, *AtPP2CF1oe*, and *ABI1oe* plants in the presence of the indicated ABA concentrations. Seed germination rate is expressed as the percentage of developed green and expanded cotyledons at 5 d after stratification. Values represent the mean ± SE of six independent experiments. Different letters above the bars indicate statistically significant differences between the lines in the presence of the indicated ABA concentrations, assessed by one-way ANOVA with Tukey-Kramer multiple comparison tests at $P < 0.05$. (D) Water loss from detached aerial parts of 3-week-old WT, *AtPP2CF1oe*, and *ABI1oe* plants. Water loss is expressed as the percentage of initial fresh weight. Values represent the mean ± SD of three independent experiments.

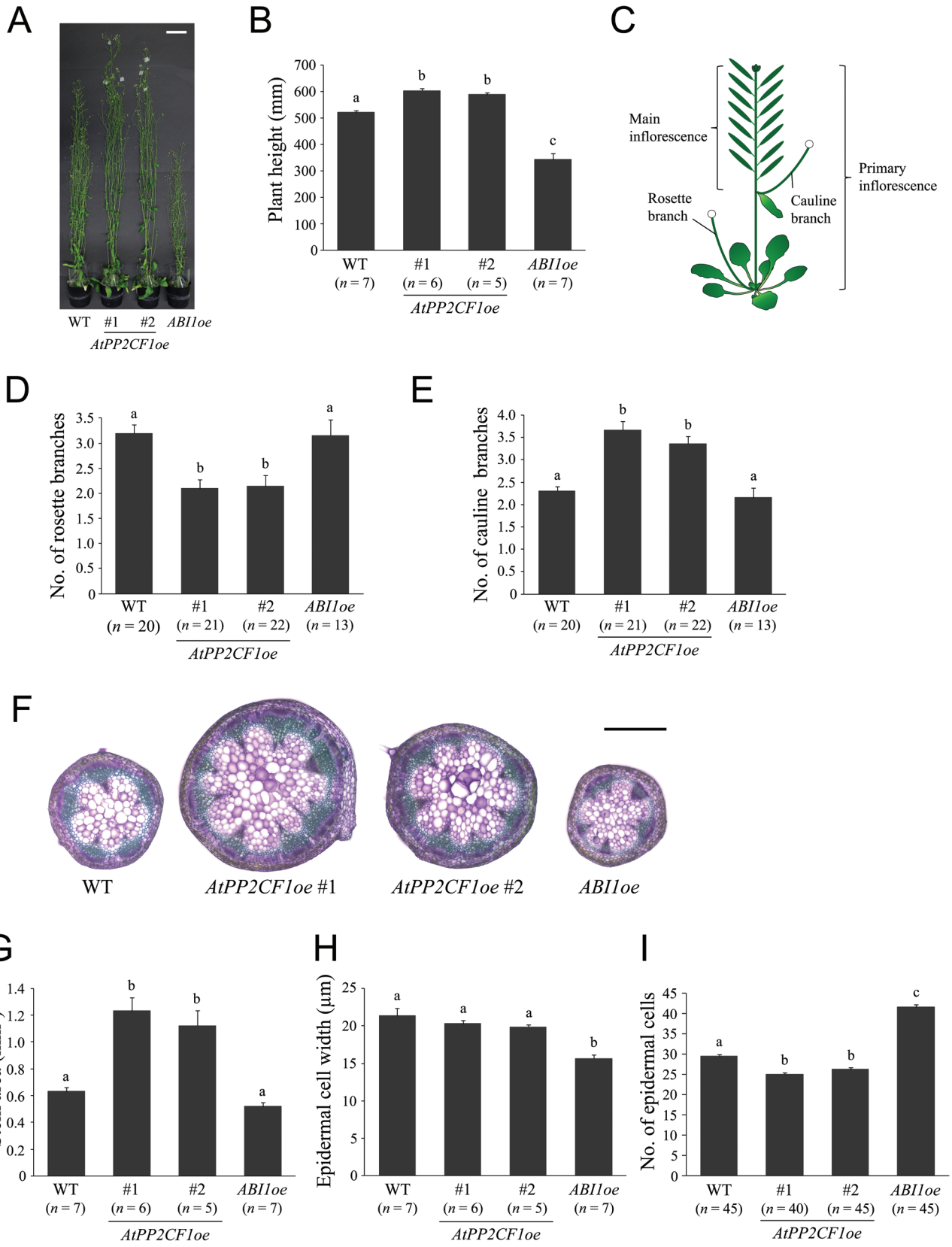

Fig. 5. *AtPP2CF1oe* plants exhibited increased inflorescence stem growth. (A) Nine-week-old wild-type (WT), *AtPP2CF1oe* (#1 and #2), and *ABI1oe* plants. (B) Height of 9-week-old plants. (C) Schematic representation of *Arabidopsis* inflorescence stems. (D, E) Number of rosette branches (D) and cauline branches on primary inflorescence (E). *Arabidopsis* plants grown until global proliferative arrest stage (Hensel *et al.*, 1994) were used for measurements. Short, thin rosette branches <10 cm in length, which occurred infrequently, were excluded from the counts. (F–I) Basal parts (20 mm from the rosette base) of primary inflorescence stems in 9-week-old plants were used for observations and measurements. (F) Transverse primary inflorescence stem sections from WT, *AtPP2CF1oe*, and *ABI1oe* plants. Sections were 100-μm thick and stained with toluidine blue. (G–I) Stem area (G) and epidermal cell width (H) and number (I). Stem epidermal cell width was determined as the stem circumference divided by the epidermal cell number

and led to an increase in dry weight of the overexpressing plants (aerial parts excluding seeds) by a factor of 1.49 compared to wild-type plants (Figs 5 and 6).

Microscopic observations of cross-sections of primary inflorescence stems revealed that the stem area in *ABI1oe* plants was the same as that in wild-type plants (Fig. 5F, G). However, the width of epidermal cells in *ABI1oe* inflorescence stems was reduced by 27% relative to the wild type, indicating increased cell division in the radial and circumferential directions in these stems (Fig. 5F–H). In contrast, stem area in *AtPP2CF1oe* was much larger than that in wild-type plants (Fig. 5F, G). *AtPP2CF1oe* inflorescence stems showed normal organization with no obvious differences in the size, shape, or degree of compactness of cells, reflecting increased cell division in the radial and circumferential directions in these stems (Fig. 5F, H).

Next, we examined the number of epidermal cells per unit stem surface (Fig. 5I and Supplementary Fig. S9). In *ABI1oe* inflorescence stems, the number of epidermal cells was increased by ~1.41-fold compared to wild-type plants (Fig. 5I). This increase was almost equal to the increase in cell numbers in the circumferential direction (37%) (Fig. 5H, I), suggesting that epidermal cells in *ABI1oe* inflorescence stems did not exhibit significant changes in a longitudinal direction. These observations suggested that the shorter stem phenotype of *ABI1oe* might be primarily a result of decreased levels of longitudinal cell-division activity. In contrast, in *AtPP2CF1oe* plants, epidermal cell numbers were substantially decreased (by 11–15%) compared with wild-type plants (Fig. 5I). These results, together with the finding of no differences in width of stem epidermal cells between wild-type and *AtPP2CF1oe* plants, indicated that stem epidermal cells in *AtPP2CF1oe* plants elongated in a longitudinal direction. The increased longitudinal length of *AtPP2CF1oe* stem epidermal cells corresponded to increased plant height (Fig. 5B, I), revealing that the promotion of *AtPP2CF1oe* stem height may result primarily from cell elongation rather than cell division.

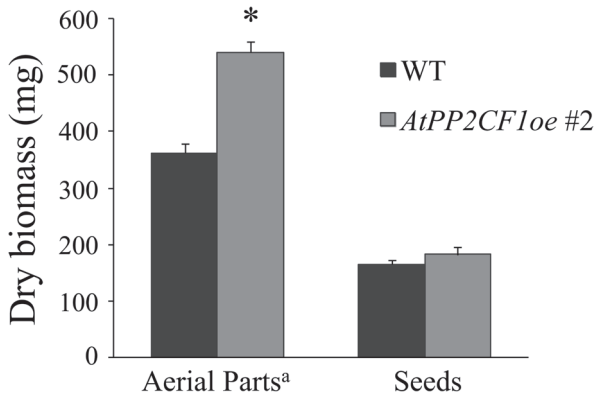

Fig. 6. Overexpression of *AtPP2CF1* enhanced biomass production in plants. Dry biomass determination was performed as described in the Materials and methods. Values represent the mean ± SD for $n = 4$. [a] Aerial plant parts did not include root tissues or seeds. * Significantly different at $P < 0.01$ (Student's t-test).

AtPP2CF1 *caused a slightly late-flowering phenotype in the overexpressing lines*

Functional loss of flowering-time genes *SOC1* and *FUL* has been reported to cause increased inflorescence stem thickness as a result of enhanced secondary growth (Melzer *et al.*, 2008); we investigated flowering time in *AtPP2CF1oe* and *ABI1oe* lines in this context. The *phyB* single and *cry2 phyB* double mutants were also included as controls for early- and late-flowering phenotypes, respectively (Mockler *et al.*, 1999). Under our growth conditions, *AtPP2CF1oe* and *ABI1oe* plants had the same flowering time and flowered significantly earlier than *cry2 phyB* plants (about 10 d earlier with two to three fewer leaves) (Fig. 7). However, both transgenic lines flowered slightly later than wild-type plants (about 3 d later with three to four more leaves), indicating that overexpression of *AtPP2CF1* or *ABI1* conferred slightly late flowering (Fig. 7).

These observations led us to wonder whether there is a relationship between flowering time and stem enlargement in these overexpressing lines. We next observed cross-sections of young primary inflorescence stems of *AtPP2CF1oe*, *ABI1oe*, and flowering mutant plants of the same developmental size rather than age (see Materials and methods for details). Stem area in the late-flowering *cry2 phyB* mutant was significantly larger than that in wild-type plants, while that of the early-flowering *phyB* mutant was substantially smaller (Fig. 8). Relative to the wild-type, phenotypes of young *AtPP2CF1oe* and *ABI1oe* inflorescence stems followed qualitatively similar trends to those seen in corresponding 9-week-old plants (Figs 5 and 8). Remarkably, despite the weaker late flowering of *AtPP2CF1oe* compared to *cry2 phyB*, *AtPP2CF1oe* plants had significantly thicker inflorescence stems than *cry2 phyB* plants (Fig. 8). Taken together, our data suggest that the enhanced stem growth and development of *AtPP2CF1oe* plants cannot be explained solely by the slight delay in flowering time, highlighting the functional significance of *AtPP2CF1* in transverse stem cell division and enlargement at the primary growth stage.

AtPP2CF1oe *plants exhibited normal fertility and seed set*

Reduced fertility in plants has been reported to cause cessation of global proliferative arrest of the inflorescence meristem, thereby increasing inflorescence stem growth (Hensel *et al.*, 1994). To test whether this was the case for

in transverse stem sections. The number of epidermal cells (not including guard cells) per unit stem epidermal area (1 mm long and 100 μm wide) was counted (see also Supplementary Fig. S9). Scale bars: 50 mm (A); 500 μm (F). All values represent the mean ± SE. Different letters above bars indicate statistically significant differences between the lines, assessed by one-way ANOVA with Tukey-Kramer multiple comparison tests at $P < 0.05$ (B, D) and $P < 0.01$ (E, G–I).

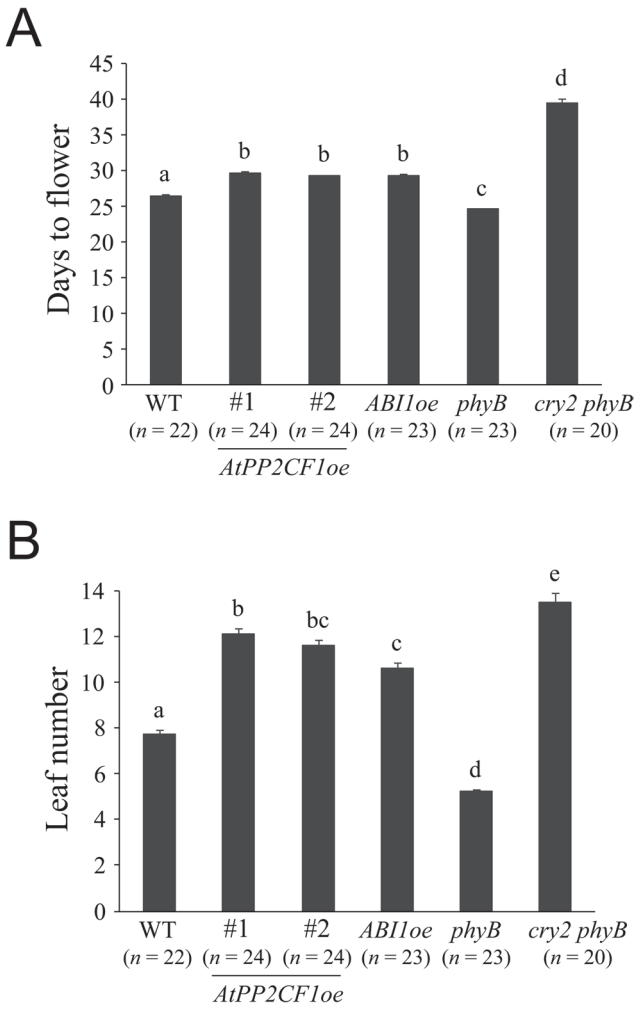

Fig. 7. Flowering time of *AtPP2CF1oe*, *ABI1oe*, *phyB*, and *cry2 phyB* plants. Flowering time was determined by counting the days to flower (A) and leaf number (B). Values represent the mean ± SE. Different letters above bars indicate statistically significant differences between the lines, assessed by one-way ANOVA with Tukey-Kramer multiple comparison tests at $P < 0.01$.

AtPP2CF1oe plants, we analysed the effect of overexpression of *AtPP2CF1* on fertility, expressed as the average number of seeds per silique on the main inflorescence. In two independent *AtPP2CF1oe*-line plants, average seed numbers per silique and seed weight were highly similar to the wild type, indicating that the fertility of *AtPP2CF1oe* plants was normal (Table 1). In contrast, *ABI1oe* plants showed significantly reduced seed production compared with the wild type (Table 1). Thus, at least for *AtPP2CF1oe* and *ABI1oe* plants, there was no association between inflorescence stem growth and fertility phenotype.

AtPP2CF1 *exhibited different expression patterns than its most closely related paralogues*

AtPP2CF1, *At5g27930*, and *At3g16800* form a small clade within subfamily E PP2Cs (Supplementary Fig. S1). A previous report (Xue *et al.*, 2008) and a Plant Genome Duplication Database (PGDD) (Lee *et al.*, 2012) search revealed that this small clade developed through segmental chromosome duplication events (Supplementary Fig. S10). To confirm whether these genes underwent functional diversification after these events, their developmental expression profiles were compared. RT-qPCR analysis revealed that *At5g27930* shared a similar expression pattern with *AtPP2CF1*, while *At3g16800* was ubiquitously expressed in all tissues, with higher levels of expression detected in the roots (Figs 1B and 9A, B).

Next, to investigate the tissue- or cell-type-specific expression patterns of *At5g27930* and *At3g16800*, we generated transgenic *Arabidopsis* plants expressing the GUS reporter gene under the transcriptional control of each gene's promoter (Fig. 9C–O and Supplementary Fig. S4). Although RT-qPCR analysis revealed similar expression patterns for *AtPP2CF1* and *At5g27930*, GUS staining revealed that the expression profiles of these *AtPP2CF1* paralogues were different from those of *AtPP2CF1* (Figs 1B–I and 9). As shown in Fig. 9C–I, GUS activity derived from the *At5g27930* promoter was detected in mesophyll cells in the leaves, sepals, ovaries, guard cells, trichomes, hypocotyls, stamen filaments, and all root tissues except for root tip regions. Moreover, *At5g27930* expression was detectable at low levels in vascular tissues (Supplementary Fig. S4). In contrast, strong GUS activity derived from the *At3g16800* promoter was observed in all root tissues except for root tip regions (especially the root vasculature), vascular tissues of the leaves and hypocotyls, and trichomes; the style and vascular tissues of sepals and petals exhibited only weak GUS activity (Fig. 9J–O and Supplementary Fig. S4). Taken together, these results suggest that *AtPP2CF1*, *At5g27930*, and *At3g16800* have completely divergent expression profiles during seedling development, indicating their sub- or neofunctionalization.

Discussion

In this study, we report a new *Arabidopsis* PP2C isoform, AtPP2CF1, as a member of PP2C subfamily E. *AtPP2F1* encoded an ABA-inducible, functional PP2C. However, our evidence suggests that the physiological roles of AtPP2CF1 in plant cells differ from those of subfamily A PP2Cs, whose gene expression is also ABA-inducible (Goda *et al.*, 2008).

Higher plants possess a larger number of PP2C genes than mammals as a result of chromosomal segment and tandem duplication events (Schweighofer *et al.*, 2004; Xue *et al.*, 2008; Singh *et al.*, 2010), allowing for great functional diversification and variation in expression patterns, subcellular localization, and substrate specificity. Indeed, increasing evidence has indicated that subfamily A PP2Cs are involved in the ABA signal transduction pathway as key negative regulators with different expression and subcellular localization profiles (Saez *et al.*, 2004; Nishimura *et al.*, 2007; Umezawa *et al.*, 2009; Zhang *et al.*, 2012). Through similar genomic rearrangement events, *AtPP2CF1*, *At5g27930*, and *At3g16800* represent a small clade within subfamily E (Xue *et al.*, 2008). Furthermore, these three genes were expressed with partial overlap but with distinct tissue- and cell-specific and ABA-responsive patterns, indicating the sub- or neofunctionalization of each gene.

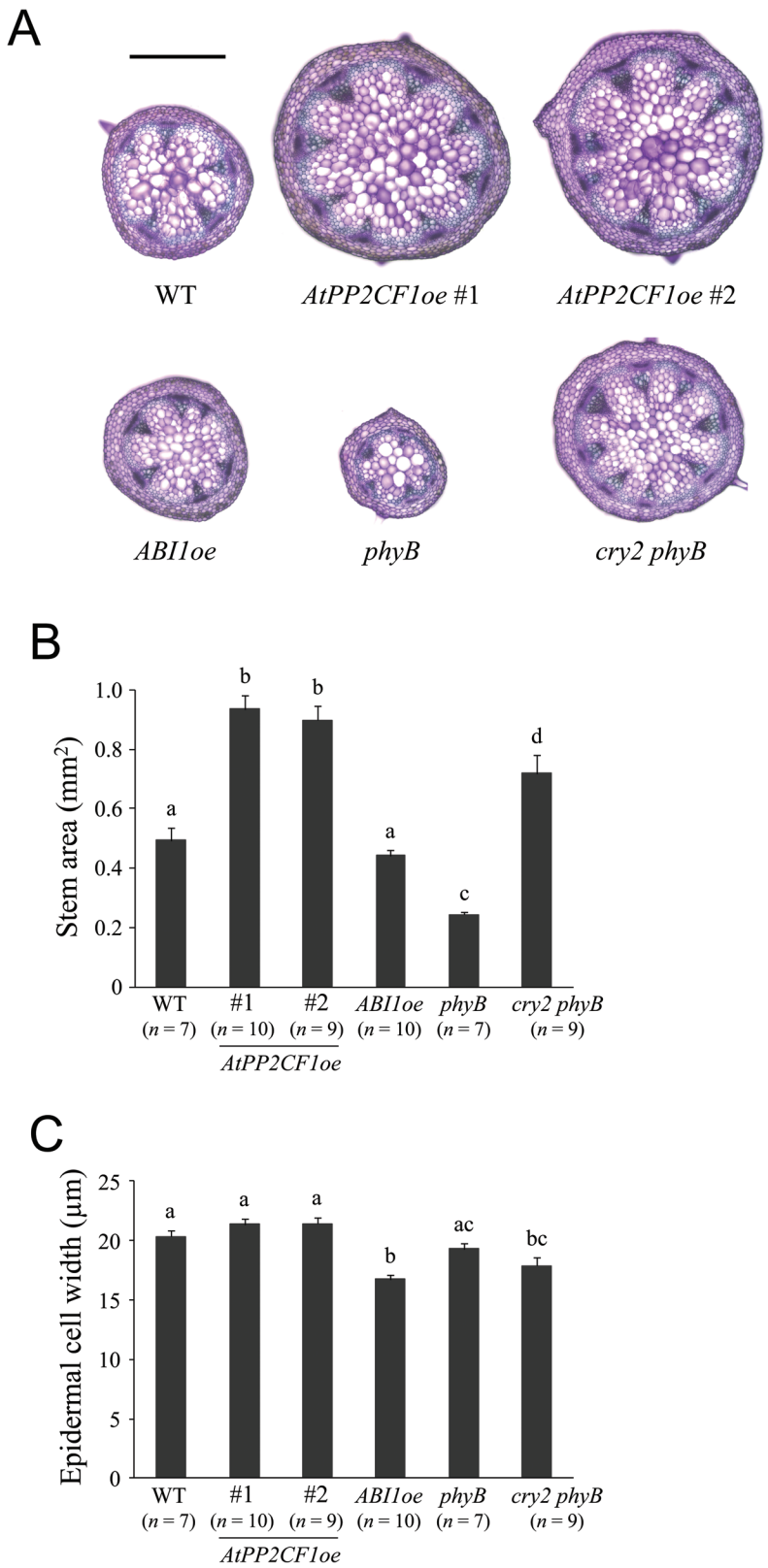

Fig. 8. Comparison of young inflorescence stem of *AtPP2CF1oe*, *ABI1oe*, *phyB*, and *cry2 phyB* plants. Basal parts (10 mm from the rosette base) of primary inflorescence stems that reached a length of 10–15 cm were used for the observations and measurements. (A) Transverse primary inflorescence stem sections from wild-type (WT), *AtPP2CF1oe* (#1 and #2), *ABI1oe*, *phyB*, and *cry2 phyB* plants. Sections were 100-μm thick and stained with toluidine blue. Scale bar: 500 μm. (B, C) Stem area (B) and epidermal cell width (C). Stem epidermal cell width was determined as the stem circumference divided by the epidermal cell number in transverse stem sections. Values represent the mean ± SE. Different letters above bars indicate statistically significant differences between the lines, assessed by one-way ANOVA with Tukey-Kramer multiple comparison tests at $P < 0.05$.

Table 1. *Fertility and seed set of* AtPP2CF1oe *and* ABI1oe *plants*[a]

Line	Number of plants	Average seed number per silique[b]	Average seed weight (μg)[c]
WT	20	34.6 ± 1.8*	18.99 ± 0.46*,†
AtPP2CF1oe #1	21	36.5 ± 1.4*	17.60 ± 0.48*
AtPP2CF1oe #2	22	34.5 ± 1.7*	17.63 ± 0.43*
ABI1oe	13	25.9 ± 2.4†	20.19 ± 0.27†

[a] The primary inflorescence stems of *Arabidopsis* plants grown until global proliferative arrest stage (Hensel *et al.*, 1994) were used to determine, on the main inflorescence, the number of siliques (containing at least one seed), infertile ovaries, and arrested buds; and seeds in each silique (see also Fig. 5C). [b] Average seed number per silique was determined as the total number of seeds on the main inflorescence divided by the number of siliques. [c] Average seed weight was calculated using 50 seeds from each plant. Values are means ± SE. Different superscript symbols (*, †) indicate statistically significant differences between lines, assessed by one-way ANOVA with Tukey-Kramer multiple comparison tests at $P < 0.05$.

Here, we provide evidence that the substrate specificity of AtPP2CF1 may differ from that of ABI1. First, in contrast to ABI1, AtPP2CF1 could not rescue the yeast *ptc1*. Second, although heterogeneous, AtPP2CF1 could not interact with molecules that signal up- or downstream of subfamily A PP2Cs (i.e. PYR/PYL/RCAR receptors and SnRK2s). Structural modelling analyses provided a plausible explanation for this property of AtPP2CF1. For example, it was observed that a protrusion caused by a unique two-amino acid insertion in the β3-α1 loop of consensus motif 4 resulted in an important structural perturbation of the interaction with PYR/PYL/RCAR receptors. Furthermore, it has been reported that Glu142 in the active site of ABI1 directly interacts with PYL1 (Miyazono *et al.*, 2009; Yin *et al.*, 2009). However, AtPP2CF1 has a Gln residue (Gln76) in the corresponding position, a common characteristic of subfamily E PP2Cs. Although AtPP2CF1 has a conserved Trp246 residue at the position corresponding to Trp300 in ABI1, the function of which is to recognize PYR/PYL/RCAR receptors and (+)-ABA, the significant distortion of the AtPP2CF1-Trp246 indole ring compared to its counterpart residue in ABI1 causes steric hindrance and prevents these receptors from binding. These data suggested that AtPP2CF1 may function differently from subfamily A PP2Cs.

Arabidopsis plants overexpressing subfamily A PP2Cs have been reported to exhibit an ABA-insensitive phenotype (Saez *et al.*, 2004; Kuhn *et al.*, 2006; Robert *et al.*, 2006; Nishimura *et al.*, 2010; Zhang *et al.*, 2012). In contrast, overexpression of AtPP2CF1 in *Arabidopsis* caused the opposite effect in seed germination and leaf evaporation assays. Furthermore, *AtPP2CF1oe* plants showed increased biomass production, in direct contrast with transgenic plants overexpressing subfamily A PP2Cs, including *ABI1oe* plants (Robert *et al.*, 2006; Nishimura *et al.*, 2010). These phenotypic differences are caused by differences in the biochemical and physiological functions of the various PP2Cs in plant cells.

The plant hormone ABA has been defined as a growth promoter under non-stress conditions, but is well known to act as a growth inhibitor under stress conditions such as drought and salinity, through the precise regulation of seed dormancy, seedling development, and stomatal behaviour (Sharp and LeNoble, 2002; Verslues and Zhu, 2007; Cutler *et al.*, 2010). For example, ABA-deficient mutants such as *aba1* and *aba2/gin1* display significant reductions in size, which is especially pronounced in leaves, inflorescence stems, and flowers, as a result of reduced cell numbers and expansion; this size reduction is observed even under non-stress conditions (i.e. humidity near saturation) (Cheng *et al.*, 2002; Barrero *et al.*, 2005). Furthermore, ABA-insensitive plants, including *srk2.2/2.3/2.6* triple mutants and transgenic lines overexpressing subfamily A PP2Cs, show a similar stunted phenotype, even under high RH (Robert *et al.*, 2006; Fujii and Zhu, 2009; Nishimura *et al.*, 2010). Thus, ABA plays an essential role in the promotion of leaf and stem development. Recent studies have demonstrated that PYR/PYL/RCAR receptors can be divided into two distinct subclasses, one comprising dimeric receptors with a lower affinity for ABA and the other comprising monomeric receptors with a significantly higher affinity for ABA (Dupeux *et al.*, 2011; Hao *et al.*, 2011). It has also been proposed that monomeric receptors may be essential for regulating basal activation of the ABA signal transduction pathway under non-stress conditions, while dimeric receptors may play a major role in the stress response under adverse environmental conditions, reinforcing the hypothesis that ABA has two distinct, opposing actions (Dupeux *et al.*, 2011; Hao *et al.*, 2011).

In the current study, we demonstrated that *AtPP2CF1* expression was ABA-inducible and could be observed in young tissues such as root tips and the basal regions of young developing leaves that exhibit rapid cell division. Intriguingly, accumulation of *AtPP2CF1* transcripts was shown to increase significantly in *gra-D* mutants, which develop large leaves with drastically increased cell numbers (Horiguchi *et al.*, 2009). Also, *AtPP2CF1oe* inflorescence stems had a markedly different phenotype from those seen in *ABI1oe* plants. *ABI1* overexpression reduced transverse stem cell enlargement and longitudinal stem cell division in inflorescence stems. In contrast, overexpression of *AtPP2CF1* led to increased transverse stem cell division and longitudinal stem cell elongation, in turn leading to increased stem height and width, and greater biomass production. Taken together, our findings suggest that *AtPP2CF1* may function as a growth-promoting factor in ABA signal transduction pathways under non-stress conditions, and may be modulated through interactions with factors downstream of monomeric PYR/PYL/RCAR receptors or with other or still-unidentified ABA receptors. It has recently been reported that ABA regulates branching by restricting the outgrowth of buds to form rosette branches (Reddy *et al.*, 2013). We also found that *AtPP2CF1oe*-line plants showed reduced rosette branches compared with wild-type and *ABI1oe* plants, supporting the idea that AtPP2CF1 might function as a positive signal transducer in ABA signalling under non-stress conditions.

Plant growth is influenced by both intrinsic genetic and extrinsic environmental cues. Despite its importance, the complex genetic and molecular networks underlying plant growth

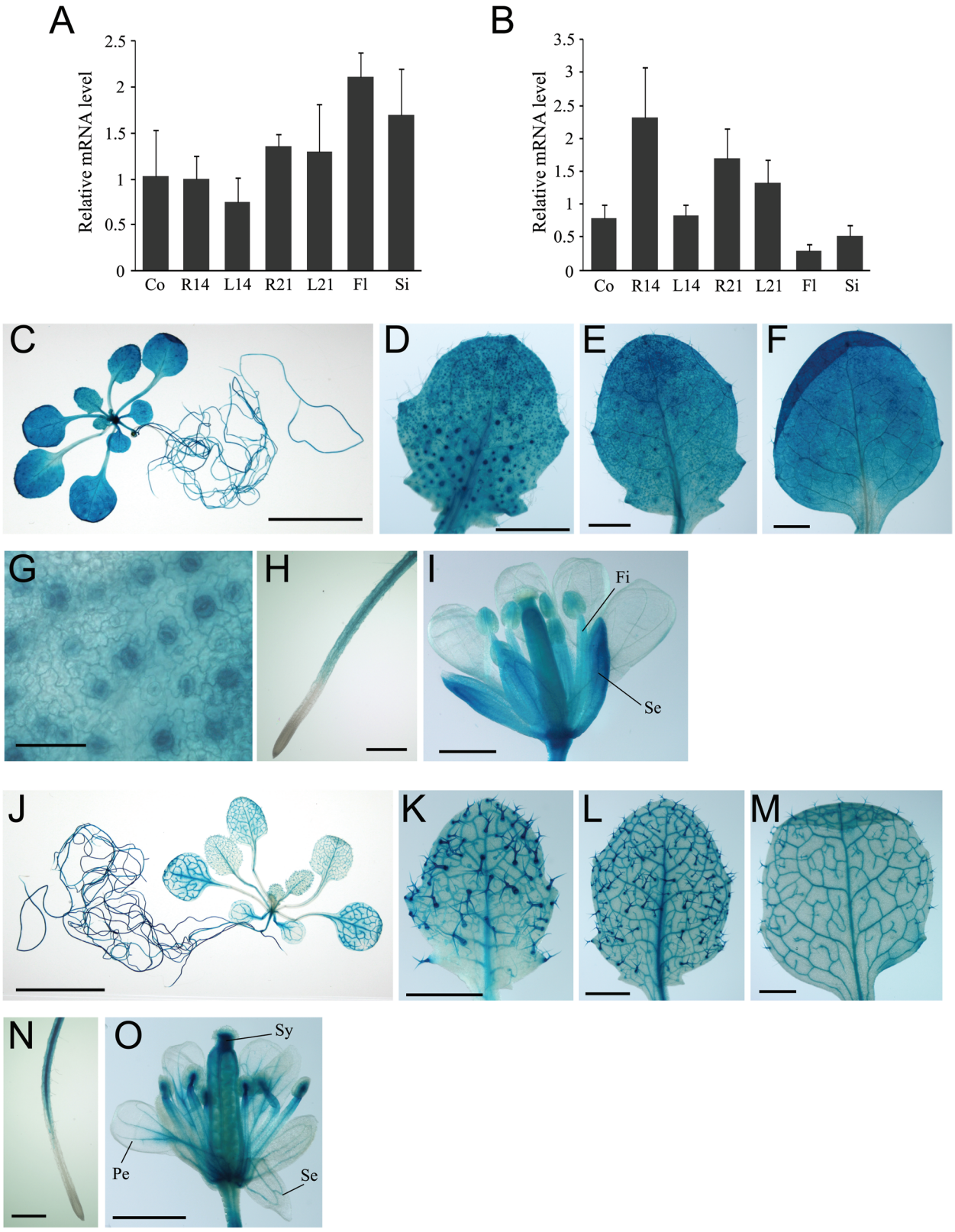

Fig. 9. Spatial and temporal regulation of *At5g27930* and *At3g16800* expression. *Arabidopsis* plants were germinated aseptically on MS medium with gellan gum. At 21 d after germination, seedlings were transferred to soil. (A, B) Expression of *At5g27930* (A) and *At3g16800* (B) transcripts. Total RNA from different tissues of wild-type *Arabidopsis* plants was isolated and subjected to RT-qPCR. The expression ratios of *At5g27930* and *At3g16800* to *UBC9* were calculated for each sample. Values represent the mean ± SD of three independent experiments. Co, 7-d-old cotyledons; R14, 14-d-old roots; L14, 14-d-old first and second rosette leaves; R21, 21-d-old roots; L21, 21-d-old first to fourth rosette leaves; Fl, flowers; Si, siliques. (C–O) Histochemical analysis of GUS activity in *Arabidopsis pAt5g27930:GUS* (C–I) and *pAt3g16800:GUS* (J–O) transgenic plants. (C, J) A 21-d-old transgenic seedling. (D–F, K–M) A developmental series of rosette leaves ranging from young (D, K) to old (F, M) within a 21-d-old transgenic seedling. (G) Guard cells of young leaves. (H, N) Roots. (I, O) Flowers. Fi, filament; Pe, petal; Se, sepal; Sy, style. Scale bars: 10 mm (C, J); 1 mm (D–F, I, K–M, O); 500 μm (H, N); 50 μm (G).

processes are poorly understood. Although we propose a potentially important functional role of AtPP2CF1 in plant biomass production, definitive proof of this role is still lacking. Nevertheless, AtPP2CF1 may represent a useful tool for gene manipulation to engineer increased biomass in crop plants.

Supplementary Material

Supplementary data are available at *JXB* online.

Supplementary Method S1. PCR templates for plasmid construction.

Supplementary Method S2. Construction of plasmids for the establishment of transgenic *Arabidopsis* plants.

Supplementary Method S3. Construction of plasmids for the yeast *ptc1* complementation test.

Supplementary Method S4. Construction of plasmids for purification of AtPP2CF1 and ABI1.

Supplementary Method S5. Y2H assays.

Supplemental Table S1. Gene-specific primers used in RT-qPCR.

Supplementary Fig. S1. Phylogenetic analysis of *Arabidopsis* PP2Cs belonging to subfamilies E and L.

Supplementary Fig. S2. Sequence alignment of conserved consensus motif 4 in all *Arabidopsis* PP2Cs.

Supplementary Fig. S3. Time course of subfamily E PP2C mRNA expression in aerial parts of wild-type *Arabidopsis* plants treated with ABA.

Supplementary Fig. S4. Histochemical analysis of GUS activity in transgenic *Arabidopsis* plants *pAtPP2CF1:GUS*, *pAt3g16800:GUS*, and *pAt5g27930:GUS*.

Supplementary Fig. S5. Multiple sequence alignments of the predicted phosphatase catalytic domain in AtPP2CF1 with those in PTC1 and ABI1.

Supplementary Fig. S6. AtPP2CF1 did not interact with PYR/PYL/RCAR receptors or with SnRK2 kinases in a Y2H assay.

Supplementary Fig. S7. Homology-based structural modelling of AtPP2CF1.

Supplementary Fig. S8. Kinematic analysis of the height of wild-type (WT), *AtPP2CF1oe* (#1 and #2), and *ABI1oe* plants.

Supplementary Fig. S9. Safranin-stained epidermises peeled from primary inflorescence stems of wild-type (WT), *AtPP2CF1oe* (#1 and #2), and *ABI1oe* plants.

Supplementary Fig. S10. Segmental chromosomal duplication regions of *AtPP2CF1*.

Acknowledgements

We would like to thank Arisa Tamura, Chie Sazuka, Masayo Suzuki, Yuriko Nakano, Miyu Miyachi, Megumi Sakai, and Ritsuko Kitagawa for technical assistance and Dr Minoru Hirano and Dr Hidenori Tanaka (Toyota Central R&D Labs. Inc.) for helpful discussions. We also thank Dr Toshinori Kinoshita (Nagoya University) for providing the *phyB-9* mutant, Dr Tomonao Matsushita (Kyushu University) for providing the *cry2-1 phyB-9* double mutant, and the RIKEN BRC (through the National Bio-Resource Project of the MEXT, Japan) for providing RIKEN *Arabidopsis* full-length (RAFL) cDNA clones developed by the plant genome project of RIKEN Genomic Sciences Center.

References

Barrero JM, Piqueras P, González-Guzmán M, Serrano R, Rodríguez PL, Ponce MR, Micol JL. 2005. A mutational analysis of the *ABA1* gene of *Arabidopsis thaliana* highlights the involvement of ABA in vegetative development. *Journal of Experimental Botany* **56,** 2071–2083.

Bertauche N, Leung J, Giraudat J. 1996. Protein phosphatase activity of abscisic acid insensitive 1 (ABI1) protein from *Arabidopsis thaliana*. *European Journal of Biochemistry* **241,** 193–200.

Bhaskara GB, Nguyen TT, Verslues PE. 2012. Unique drought resistance functions of the *highly ABA-induced* clade A protein phosphatase 2Cs. *Plant Physiology* **160,** 379–395.

Brock AK, Willmann R, Kolb D, Grefen L, Lajunen HM, Bethke G, Lee J, Nürnberger T, Gust AA. 2010. The Arabidopsis mitogen-activated protein kinase phosphatase PP2C5 affects seed germination, stomatal aperture, and abscisic acid-inducible gene expression. *Plant Physiology* **153,** 1098–1111.

Cheng W-H, Endo A, Zhou L *et al.* 2002. A unique short-chain dehydrogenase/reductase in Arabidopsis glucose signaling and abscisic acid biosynthesis and functions. *The Plant Cell* **14,** 2723–2743.

Clough SJ, Bent AF. 1998. Floral dip: a simplified method for *Agrobacterium*-mediated transformation of *Arabidopsis thaliana*. *The Plant Journal* **16,** 735–743.

Cohen PTW. 1994. Nomenclature and chromosomal localization of human protein serine/threonine phosphatase genes. *Advances in Protein Phosphatases* **8,** 371–376.

Cutler SR, Rodriguez PL, Finkelstein RR, Abrams SR. 2010. Abscisic acid: emergence of a core signaling network. *Annual Review of Plant Biology* **61,** 651–679.

Dupeux F, Santiago J, Betz K *et al.* 2011. A thermodynamic switch modulates abscisic acid receptor sensitivity. *The EMBO Journal* **30,** 4171–4184.

Fujii H, Zhu JK. 2009. Arabidopsis mutant deficient in 3 abscisic acid-activated protein kinases reveals critical roles in growth, reproduction, and stress. *Proceedings of the National Academy of Sciences, USA* **106,** 8380–8385.

Goda H, Sasaki E, Akiyama K *et al.* 2008. The AtGenExpress hormone and chemical treatment data set: experimental design, data evaluation, model data analysis and data access. *The Plant Journal* **55,** 526–542.

Hao Q, Yin P, Li W, Wang L, Yan C, Lin Z, Wu JZ, Wang J, Yan SF, Yan N. 2011. The molecular basis of ABA-independent inhibition of PP2Cs by a subclass of PYL proteins. *Molecular Cell* **42,** 662–672.

Hauser F, Waadt R, Schroeder JI. 2011. Evolution of abscisic acid synthesis and signaling mechanisms. *Current Biology* **21,** R346–355.

Hensel LL, Nelson MA, Richmond TA, Bleecker AB. 1994. The fate of inflorescence meristems is controlled by developing fruits in *Arabidopsis*. *Plant Physiology* **106,** 863–876.

Horiguchi G, Gonzalez N, Beemster GTS, Inzé D, Tsukaya H. 2009. Impact of segmental chromosomal duplications on leaf size in the *grandifolia-D* mutants of *Arabidopsis thaliana*. *The Plant Journal* **60,** 122–133.

Hubbard KE, Nishimura N, Hitomi K, Getzoff ED, Schroeder JI. 2010. Early abscisic acid signal transduction mechanisms: newly discovered components and newly emerging questions. *Genes and Development* **24,** 1695–1708.

Joshi-Saha A, Valon C, Leung J. 2011. Abscisic acid signal off the STARting block. *Molecular Plant* **4,** 562–580.

Koiwai H, Nakaminami K, Seo M, Mitsuhashi W, Toyomasu T, Koshiba T. 2004. Tissue-specific localization of an abscisic acid biosynthetic enzyme, AAO3, in Arabidopsis. *Plant Physiology* **134,** 1697–1707.

Kuhn JM, Boisson-Dernier A, Dizon MB, Maktabi MH, Schroeder JI. 2006. The protein phosphatase *AtPP2CA* negatively regulates abscisic acid signal transduction in Arabidopsis, and effects of *abh1* on *AtPP2CA* mRNA. *Plant Physiology* **140,** 127–139.

Lee T-H, Tang H, Wang X, Paterson AH. 2012. PGDD: a database of gene and genome duplication in plants. *Nucleic Acids Research* **41,** D1152–1158.

Leung J, Merlot S, Giraudat J. 1997. The Arabidopsis *ABSCISIC ACID-INSENSITIVE2* (*ABI2*) and *ABI1* genes encode homologous protein

phosphatases 2C involved in abscisic acid signal transduction. *The Plant Cell* **9,** 759–771.

Liu X, Zhu Y, Zhai H, Cai H, Ji W, Luo X, Li J, Bai X. 2012. AtPP2CG1, a protein phosphatase 2C, positively regulates salt tolerance of *Arabidopsis* in abscisic acid-dependent manner. *Biochemical and Biophysical Research Communications* **422,** 710–715.

Lu G, Wang Y. 2008. Functional diversity of mammalian type 2C protein phosphatase isoforms: new tales from an old family. *Clinical and Experimental Pharmacology and Physiology* **35,** 107–112.

Ma Y, Szostkiewicz I, Korte A, Moes D, Yang Y, Christmann A, Grill E. 2009. Regulators of PP2C phosphatase activity function as abscisic acid sensors. *Science* **324,** 1064–1068.

Maeda T, Tsai AYM, Saito H. 1993. Mutations in a protein tyrosine phosphatase gene (*PTP2*) and a protein serine/threonine phosphatase gene (*PTC1*) cause a synthetic growth defect in *Saccharomyces cerevisiae*. *Molecular and Cellular Bioliogy* **13,** 5408–5417.

Melcher K, Ng L-M, Zhou XE *et al.* 2009. A gate-latch-lock mechanism for hormone signalling by abscisic acid receptors. *Nature* **462,** 602–608.

Melzer S, Lens F, Gennen J, Vanneste S, Rohde A, Beeckman T. 2008. Flowering-time genes modulate meristem determinacy and growth form in *Arabidopsis thaliana*. *Nature Genetics* **40,** 1489–1492.

Merlot S, Gosti F, Guerrier D, Vavasseur A, Giraudat J. 2001. The ABI1 and ABI2 protein phosphatases 2C act in a negative feedback regulatory loop of the abscisic acid signalling pathway. *The Plant Journal* **25,** 295–303.

Miyazono K, Miyakawa T, Sawano Y *et al.* 2009. Structural basis of abscisic acid signalling. *Nature* **462,** 609–614.

Mockler TC, Guo H, Yang H, Duong H, Lin C. 1999. Antagonistic actions of *Arabidopsis* cryptochromes and phytochrome B in the regulation of floral induction. *Development* **126,** 2073–2082.

Nishimura N, Hitomi K, Arvai AS, Rambo RP, Hitomi C, Cutler SR, Schroeder JI, Getzoff ED. 2009. Structural mechanism of abscisic acid binding and signaling by dimeric PYR1. *Science* **326,** 1373–1379.

Nishimura N, Sarkeshik A, Nito K *et al.* 2010. PYR/PYL/RCAR family members are major *in-vivo* ABI1 protein phosphatase 2C-interacting proteins in Arabidopsis. *The Plant Journal* **61,** 290–299.

Nishimura N, Yoshida T, Kitahata N, Asami T, Shinozaki K, Hirayama T. 2007. *ABA-Hypersensitive Germination1* encodes a protein phosphatase 2C, an essential component of abscisic acid signaling in Arabidopsis seed. *The Plant Journal* **50,** 935–949.

Park S-Y, Fung P, Nishimura N *et al.* 2009. Abscisic acid inhibits type 2C protein phosphatases via the PYR/PYL family of START proteins. *Science* **324,** 1068–1071.

Reddy SK, Holalu SV, Casal JJ, Finlayson SA. 2013. Abscisic acid regulates axillary bud outgrowth responses to the ratio of red to far-red light. *Plant Physiology* **163,** 1047–1058.

Robert N, Merlot S, N'Guyen V, Boisson-Dernier A, Schroeder JI. 2006. A hypermorphic mutation in the protein phosphatase 2C HAB1 strongly affects ABA signaling in *Arabidopsis*. *FEBS Letters* **580,** 4691–4696.

Saez A, Apostolova N, Gonzalez-Guzman M, Gonzalez-Garcia MP, Nicolas C, Lorenzo O, Rodriguez PL. 2004. Gain-of-function and loss-of-function phenotypes of the protein phosphatase 2C *HAB1* reveal its role as a negative regulator of abscisic acid signalling. *The Plant Journal* **37,** 354–369.

Santiago J, Dupeux F, Round A, Antoni R, Park S-Y, Jamin M, Cutler SR, Rodriguez PL, Márquez JA. 2009. The abscisic acid receptor PYR1 in complex with abscisic acid. *Nature* **462,** 665–668.

Schweighofer A, Hirt H, Meskiene I. 2004. Plant PP2C phosphatases: emerging functions in stress signaling. *Trends in Plant Science* **9,** 236–243.

Sharp RE, LeNoble ME. 2002. ABA, ethylene and the control of shoot and root growth under water stress. *Journal of Experimental Botany* **53,** 33–37.

Shi Y. 2009. Serine/threonine phosphatases: mechanism through structure. *Cell* **139,** 468–484.

Singh A, Giri J, Kapoor S, Tyagi AK, Pandey GK. 2010. Protein phosphatase complement in rice: genome-wide identification and transcriptional analysis under abiotic stress conditions and reproductive development. *BMC Genomics* **11,** 435.

Soon F-F, Ng L-M, Zhou XE *et al.* 2012. Molecular mimicry regulates ABA signaling by SnRK2 kinases and PP2C phosphatases. *Science* **335,** 85–88.

Umezawa T, Sugiyama N, Mizoguchi M, Hayashi S, Myouga F, Yamaguchi-Shinozaki K, Ishihama Y, Hirayama T, Shinozaki K. 2009. Type 2C protein phosphatases directly regulate abscisic acid-activated protein kinases in *Arabidopsis*. *Proceedings of the National Academy of Sciences, USA* **106,** 17588–17593.

Verslues PE, Zhu JK. 2007. New developments in abscisic acid perception and metabolism. *Current Opinion in Plant Biology* **10,** 447–452.

Winzeler EA, Shoemaker DD, Astromoff A *et al.* 1999. Functional characterization of the *S. cerevisiae* genome by gene deletion and parallel analysis. *Science* **285,** 901–906.

Xue T, Wang D, Zhang S, Ehlting J, Ni F, Jakab S, Zheng C, Zhong Y. 2008. Genome-wide and expression analysis of protein phosphatase 2C in rice and Arabidopsis. *BMC Genomics* **9,** 550.

Yin P, Fan H, Hao Q, Yuan X, Wu D, Pang Y, Yan C, Li W, Wang J, Yan N. 2009. Structural insights into the mechanism of abscisic acid signaling by PYL proteins. *Nature Structural and Molecular Biology* **16,** 1230–1236.

Zhang K, Xia X, Zhang Y, Gan S-S. 2012. An ABA-regulated and Golgi-localized protein phosphatase controls water loss during leaf senescence in Arabidopsis. *The Plant Journal* **69,** 667–678.